Chalcogenide Letters

Tech Science Press

http://doi.org/10.32604/cl.2026.077900

ARTICLE

Effect of Rays on the Impedance Spectrum of Solid Solutions of the $(TlGaSe_2)_{1-x}(TlInS_2)_x$

A. A. Orujova[1], T. F. Yusibova[1], R. Sh. Agayeva[1], G. A. Ismayilbeyli[1] and N. I. Guliyev[2,*]

[1]Department of Physics and Ecology, Mingachevir State University, Mingachevir, Azerbaijan
[2]Department of Physics, Ganja State University, Ganja, Azerbaijan
*Corresponding Author: N. I. Guliyev. Email: abayramova@rambler.ru

Received: 19 December 2025; Accepted: 25 March 2026; Published: 09 May 2026

ABSTRACT: Warburg impedance models the process of diffusion of mobile ions from the electrode to the diffusion layer under a sinusoidal voltage applied at one polarity of an electrochemical cell, and the diffusion of mobile ions to the electrode at the other polarity. As a result, the process does not go beyond the diffusion layer. In this case, the diffusion of Tl^{+1} ions in the $TlInS_2$ crystal (as well as in solid solutions) after 25 Mrad irradiation is considered to be responsible for the formation of the Warburg diffusion impedance. The transition to the superionic state is confirmed by measuring the temperature dependence of electrical conductivity. It was found that the relaxation time decreases after the crystals are exposed to radiation. The complex plane diagrams were analyzed using the equivalent circuit substitution method. It has been shown that the system of solid solutions undergoes a phase transition to the superionic state after γ-irradiation.

KEYWORDS: Impedance spectroscopy; Warburg impedance; solid solutions; superionic; Tl^+ ion diffusion conductivity

1 Introduction

The study of the regularities governing the composition and structure of multicomponent semiconductors is one of the fundamental problems of modern physics. Investigating these regularities makes it possible to establish a scientific basis for the development and production of new, more efficient semiconductor materials with predetermined physical properties, thereby meeting the increasing demands of modern quantum physics and microelectronics.

Research on new semiconductor materials, especially those obtained in the form of perfect and large crystals, remains a constant focus of scientific interest. Among the wide variety of semiconductors, special attention is given to materials with layered crystal structures due to their unique properties and potential applications. Interest in such semiconductors continues to grow from both scientific and practical perspectives.

Therefore, expanding the class of layered semiconductors, producing high-quality perfect crystals, and conducting comprehensive studies of their physical properties are considered highly relevant tasks in modern semiconductor physics.

At the same time, the search for semiconductor materials with predetermined properties requires studying the influence of various additives and impurities on the physical parameters of promising compounds.

For this purpose, obtaining $TlGaSe_2$, $TlInS_2$ compounds and their solid solutions and controlling their physical parameters in a wide range is of practical importance. The aim of the present work was to study the impedance spectra of $(T\ell GaSe_2)_{1-x}(T\ell InS_2)_x$ system solid solutions irradiated with γ-quanta.

2 Materials and Methods of the Study

Single crystals of $T\ell GaSe_2$ and $T\ell InS_2$ and its compounds and their solutions were grown by the Biricman-Stockbarger method.

The essence of the Biricman-Stockbarger method is that crystallization is carried out in a temperature gradient field to form a nucleus at the boundary between the alloy and the crystal [1,2].

Ampoules with a length of 0.23–0.25 m, a diameter of 0.05–0.1 m, and a wall thickness of $(2.0–2.5)\cdot10^{-2}$ m were placed in inclined furnaces at 10–15°C in such a way that one-third of the ampoule remained in the air. The heating rate of the furnace was 0.16–0.20 K/s. In this setup, part of the chalcogen (sulfur) vapor reacts with Tl and In, while the rest condenses at the cold end of the ampoule and flows back into the reaction zone. Usually, excess chalcogen vapor increases the pressure in the ampoule in the hot zone, which creates the risk of an explosion. To prevent this, a bend was introduced in the diameter of the ampoule near the neck. This led to the formation of a kind of chalcogen bowl, which was then compressed into a liquid and did not flow into the ampoule.

The bowl itself was at a distance of $(2–3)\cdot10^{-2}$ m from the furnace outlet. In this case, evaporation of chalcogen occurred, and when the pressure in the ampoule decreased, it entered the reaction zone, that is, the same part of the chalcogen that was in the reaction zone. In this case, there was no need to cool the ampoule. During the reaction of the components, the ampoules gradually moved into the furnace. To mix the alloy during the interaction, the ampoules were bent along their axes, and the cooling of the material was carried out in a furnace with the furnace turned off.

$(T\ell GaSe_2)_{1-x}(T\ell InS_2)_x$ system solid solutions were synthesized by a single-temperature synthesis method. Since there was no interaction of the components with quartz during the synthesis process, the purity of the samples was achieved.

After cleaning, the quartz ampoules used in the synthesis processes were filled with stoichiometric amounts of components weighed on an analytical balance and vacuumed ($1.33 \cdot 10^{-2}$ Pa to pressure) and sealed with propane-oxygen gas.

When the mixture is melted, the melt is then maintained at a certain temperature by periodic stirring; after that, the ampoule is cooled to a temperature approximately 0.03 K below the melting temperature (T_m) of the synthesized material, where T_m ranges from 100 to 150 K. Then, the furnace is turned off and the cooling of the synthesized material is carried out in the turned off furnace.

The γ-25 gamma device (radiation research device) consists of radiation sources made of C_0^{60} isotope and is intended for physical, chemical, and biological research. In the non-operating state, the radiation sources of the device are submerged under water.

This is to protect against gamma rays. In the working state, the sources of the system are raised under water to the surface of the working table and cover the cylindrical surface. Thus, the irradiation of the samples is carried out by the working chamber. The system of the γ-source consists of tubes and cassettes. Cylindrical rods made of cobalt isotope are placed inside them. This cylinder is limited by holders at the bottom and top. The tubes are placed along the circumference. Therefore, they have symmetry.

The impedance spectroscopy method was initially developed for use in electrochemical systems. Later, its effectiveness in the investigation of solid materials was recognized. In the 1970s, this method became

widely applied in experimental solid-state physics, particularly during the period of rapid development in the study of solid-state ionic materials [3].

In practice, the method consists in measuring the frequency dependence of the real Z' and imaginary Z'' parts of the complex impedance $Z = Z' - j\,Z''$ in alternating current, where j is an imaginary unit. Generally speaking, impedance spectroscopy can also be represented by the complex permittivity $\gamma = 1/Z$, the electrical modulus $M = 1/\varepsilon$, and the dielectric permittivity $\varepsilon = \gamma/(j\omega C_0)$, where C_0—is the geometric capacitance of the sample. The graph or impedance spectrum represented in the coordinates Z'' (Z'), called the hodograph, visually shows the experimental results. The shape of the equivalent circuit corresponds to a certain physical model of the sample [4–9].

In the hodograph analysis, each of the corresponding additions to the impedance *Zgb* from the core volume *Zb* and the inter-core boundaries can be described within the equivalent circuit approximation of a parallel *RC*-contour. The shape of the corresponding hodograph, determined by the ratio of the parameters of the two contours, will be two consecutive semicircular structures for a given significant difference in time constants. Such impedance spectra have often been observed in experiments on ceramic samples [10–12].

As is always the case in the impedance spectrum of a polycrystal, the volume and boundaries of the crystal correspond to two contours (Fig. 1). In contrast, the shape of the hodograph often appears as a series of arcs that change frequently. On the one hand, taking into account the above-described ideas regarding the microstructure of the polycrystal, the analysis of the data can be carried out using an equivalent circuit with the parameters R_b, C_b, R_{gb}, and C_{gb}, which most conveniently approximate the hodograph. On the other hand, the advantage of such an approach is questionable in the absence of direct experimental evidence for the existence of two contours. In addition, it is considered expedient to choose a simpler approximate equivalent circuit: a single RC circuit is constructed with effective parameters R and C representing the resistance and capacitance of the sample, connected in series (Fig. 1).

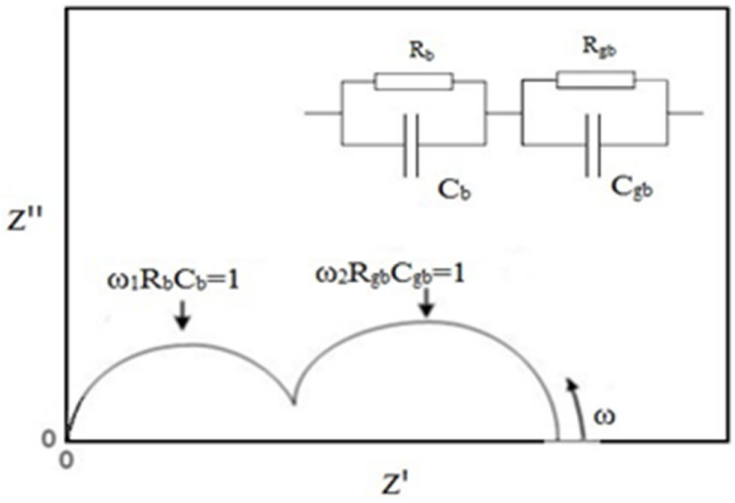

Figure 1: Impedance hodograph model of a polycrystalline sample and its equivalent replacement scheme.

Unlike the basic two-phase approximation, the Maxwell-Wagner model accounts for the actual distribution of current within the sample. Generally, the capacitance tends to decrease as the frequency increases, while at low frequencies its effective value can become anomalously high. For frequencies below 10^{12} Hz, such effects are not expected in any of the three known polarization mechanisms—ionic, electronic, or orientational—since these involve fast electronic processes. Several studies, including [13], demonstrate that even in the absence of dipole moments, due to the properties of the crystal lattice (for

example, in ferroelectric perovskite systems), an unusually high effective capacitance may be observed. This behavior is attributed to the inhomogeneity of the sample, which can be explained by the attenuation of charge discharge at boundaries between regions of differing conductivity, effectively forming a network of numerous capacitors.

The presence of distributed capacitance, the experimentally determined capacitance, does not allow us to interpret the characteristic properties of the sample itself and does not allow us to correctly calculate its dielectric constant using the simplest formulas for a surface capacitor. The phenomena described in the literature are called the Maxwell-Wagner effect. In the case of polycrystalline materials, such effects can arise as a result of polarization processes in the intermediate region of the crystal [13]. As the frequency of the external field increases, "freezes" weak processes of the non-uniform field in the structure.

The manifestation of the Maxwell-Wagner effect is associated with polarization processes in the contact area. The formation of a barrier capacitance at the contact can significantly change (distort) the experimental results and lead to large experimental capacitance values. Sometimes, however, questions related to the possible Maxwell-Wagner effects are not paid attention to, and the high value of the capacitance is directly related to the dielectric properties of the sample, which is also incorrect and leads to erroneous conclusions [14,15]. In this work, the authors, most likely, reviewed many articles [16–20] on the determination of the dielectric constant of the studied material, including ferroelectrics. To eliminate such errors, it is important to determine the influence of the contact on the impedance measurement results by analyzing the data obtained for various contact configurations of the studied sample and the measured parameters [21–26].

3 Results

The complex impedance and relaxation processes of solid solutions of the $(TlGaSe_2)_{1-x}(TlInS_2)_x$(0.1, 0.6, 0.8) system exposed to 25 Milliradian γ-radiation were investigated in the frequency range of $25/10^6$ Hs by the impedance spectroscopy method.

Impedance spectroscopy is widely recognized as an effective technique for investigating electrophysical processes occurring at metal contacts in ion-conducting materials. In this study, the real (Z′) and imaginary (Z′′) components of the impedance for $(TlGaSe_2)_{1-x}(TlInS_2)_x$ solid solution samples were measured. The obtained data are presented in the form of complex impedance plots (Nyquist plots), as shown in Fig. 2. The obtained dependences can be described using an equivalent circuit consisting of parallel elements. The characteristic relaxation frequencies f_{max} corresponding to the maxima of the imaginary part of the impedance (Z′′), were determined. In addition, the frequencies marking the onset of dispersion for the $(TlGaSe_2)_{1-x}(TlInS_2)_x$ solid solution samples, both before and after irradiation with a dose of 25 Mrad, are summarized in the table. According to the data, an increase in the f_{max} values is observed after irradiation. As illustrated in Fig. 2a,b, the impedance spectra of the solid solution samples form arcs in the complex plane that are slightly depressed and inclined with respect to the real axis, approaching a semicircular shape at the intersection of Z′ and Z′′.

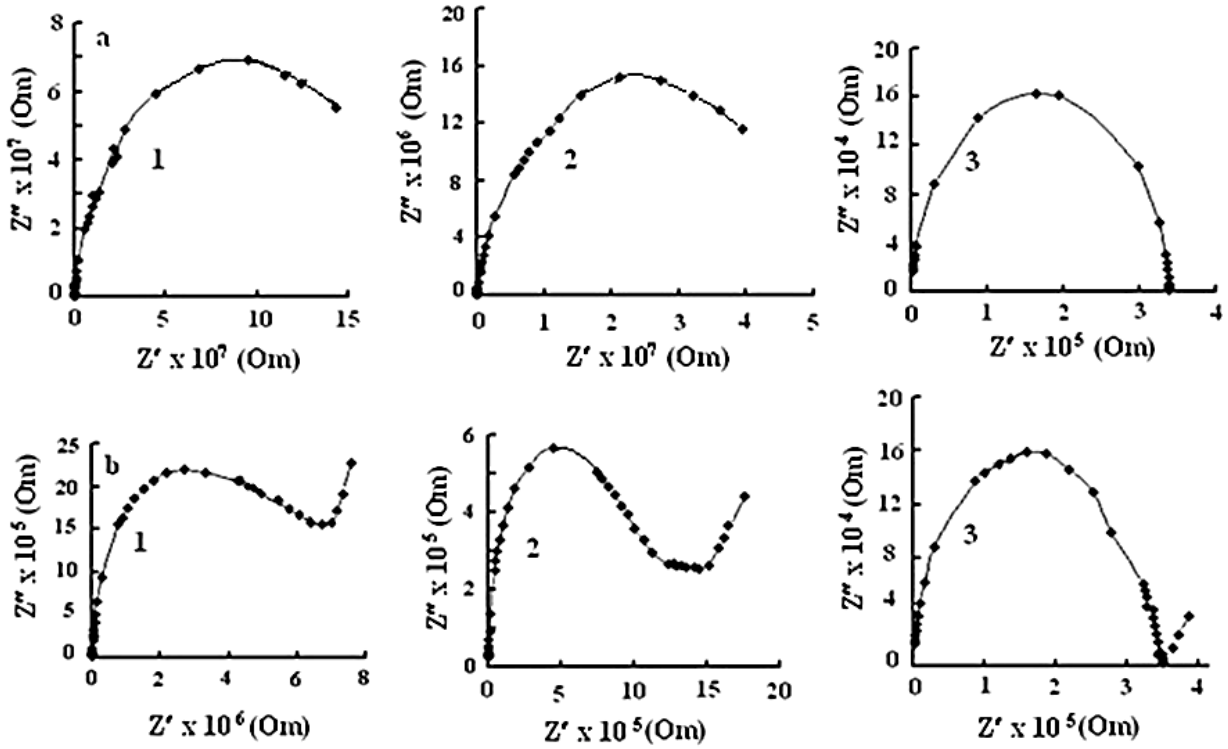

Figure 2: (Z″–Z′)—diagrams constructed in the complex plane based on the results of Z″(ω) and Z′(ω) measurements of the $(TlGaSe_2)_{1-x}(TlInS_2)_x$ solid solution (**a**)—(1) x = 0.1; (2) x = 0.8; (3) x = 0.6; after irradiation (**b**)—(1) x = 0.1; (2) x = 0.8; (3) x = 0.6.

4 Discussion

This type of behavior can be adequately represented by a parallel equivalent circuit (Fig. 3a). Under these conditions, the charge transport process is governed by a single characteristic relaxation time. The imaginary part of the impedance shows a maximum at frequencies $f_{(max)}$ corresponding to the condition $C_{eff}R_{eff}\omega_{max} = 1$, where C_{eff} and R_{eff} are the effective parameters of the equivalent circuit, $\omega_{max} = 2\pi f_{max}$ is the circular frequency. In Fig. 2, impedance hodographs are shown for the $(TlGaSe_2)_{1-x}(TlInS_2)_x$ solid solutions at x = 1, 0.8, 0.6, the measurements were performed before irradiation (curve a) and after 25 Mrad irradiation (curve b). The upper (tip) part of the hodograph arc corresponds to the resonance frequency ω_{max}.

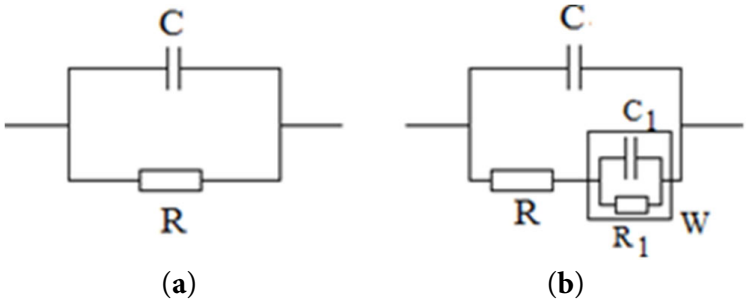

Figure 3: Equivalent scheme (**a**) before irradiation, (**b**) after 25 Mrad irradiation. W—Barburg impedance diffusion, R—sample resistance.

The calculated parameters are summarized in Table 1. The results indicate that the charge transport process is characterized by a single relaxation time, whereas the spectra obtained prior to irradiation exhibit a shape close to a semicircle centered on the real axis. Such a hodograph is typical of a homogeneous sample with relatively low resistance and non-degenerate contacts, and its corresponding equivalent circuit is presented in Fig. 3a. In contrast, the (Z″–Z′) plots obtained after irradiation with a dose of 25 Mrad display semicircular features associated with a parallel RC circuit, along with linear regions in the low-frequency range. The impedance hodographs recorded after irradiation suggest the presence of additional contributions to the conductivity, which are likely related to the diffusion transport of thallium ions near the interface between the solid electrolyte and the electrode.

Table 1: Calculated values according to $z'(\omega)$ and $z''(\omega)$ measurements.

Composition	Mrad Radiation Dose	$f_{\max}$, (kHs) max. Frequency Range	$\eta = 1/2f_{\max}$ Relaxation Time	f_{jamp}, (kHs) Amplitude Value of Frequency
$TlInS_2$	0	0.1	$1.6 \cdot 10^{-3}$	1
	25	5	$3.18 \cdot 10^{-5}$	50
$(TlGaSe_2)_{0.2}(TlInS_2)_{0.8}$	0	0.3	$5.3 \cdot 10^{-4}$	6
	25	20	$7.9 \cdot 10^{-6}$	100
$(TlGaSe_2)_{0.4}(TlInS_2)_{0.6}$	0	60	$2.65 \cdot 10^{-6}$	500
	25	70	$1.01 \cdot 10^{-6}$	600

These characteristics observed in the impedance spectra are attributed to the presence of Warburg diffusion impedance, which arises because the sinusoidal excitation of the charge carriers does not fully penetrate the diffusion layer within the applied frequency range. As a consequence of the emergence of Warburg-type behavior, the crystal is likely to undergo a transition to a superionic state following irradiation with a dose of 25 Mrad.

Based on these graphs, the effect of irradiation on the $(TlGaSe_2)_{1-x}(TlInS_2)_x$ solid solution can be explained as follows. Comparative analysis of the Nyquist ($z'' - z'$) diagrams obtained before and after irradiation in the studied $(TlGaSe_2)_{1-x}(TlInS_2)_x$ solid product system shows that serious microscopic changes occur in the internal structure of the material.

In the cases before irradiation (Fig. 2, curves a), the diameter of the semicircles is larger, which proves that the material has a high internal resistance (R_b). After irradiation (Fig. 2, curves b), a narrowing of the semicircles along the x axis is observed. This is explained by the formation of additional charge carriers (vacancies, displaced atoms or free electrons) in the crystal lattice as a result of radiation. As a result, the specific conductivity of the material increases.

The semicircular shape in the graphs indicates that the material has a uniform relaxation time (τ). The shift of the peak point of the semicircles as a result of irradiation indicates that it has a relaxation frequency ($\omega_{\max} = 1/\tau$). This is an indication that the radiation defect directly affects the polarizability of the material and the oscillation frequency of the dipoles.

The linear tails observed in the low-frequency region (right-hand side) of the post-irradiation plots (Fig. 2b), corresponding to Warburg impedance, indicate the activation of diffusion-related processes of charge carriers within the material. This behavior can be attributed to charge accumulation at the interparticle boundaries of the crystal after irradiation, which leads to the formation of additional potential barriers at the electrode–material interface.

The variation of the parameter x (from 1.0 to 0.6) indicates a different sensitivity to radiation. For example, while the resistance change is more drastic in the case of x = 1 (pure ($TlInS_2$)), the radiation resistance or response of the material is modified as the composition of the solid solution changes.

5 Conclusion

Thus, Warburg impedance describes the diffusion of mobile ions between the electrode and the diffusion layer under an applied sinusoidal potential, with ion transport occurring toward the diffusion layer at one polarity and toward the electrode at the opposite polarity. Consequently, the process remains confined within the diffusion layer. In this context, the diffusion of Tl^+ ions in the $TlInS_2$ crystal, as well as in its solid solutions after irradiation with a dose of 25 Mrad, is considered to be responsible for the emergence of Warburg-type impedance. The transition to a superionic state is further supported by the temperature dependence of the electrical conductivity, as discussed above.

It was found that the relaxation time decreases after the crystals are exposed to radiation. The (Z''–Z') complex plane diagrams were analyzed using the equivalent circuit substitution method (Fig. 3a,b).

It was shown that the $(TlGaSe_2)_{1-x}(TlInS_2)_x$ system solid solutions undergo a phase transition to the superionic state after γ irradiation.

This result constitutes a notable contribution to the field at the intersection of solid-state and radiation physics. The novelty of the present study is associated with the pronounced sensitivity of the lattice dynamics of thallium-containing semiconductors to irradiation, which leads to their transition into a qualitatively new superionic state at an irradiation dose of 25 Mrad.

Layered crystals such as $TlGaSe_2$ and $TlInS_2$ (or solid solution systems) are very interesting objects for radiation physics and solid-state electronics. The fact that superionic states are formed in these materials under the influence of radiation (for example, γ-quanta or electron flux) increases their scientific and technological importance. Both the theoretical limitations and the practical application areas of this scientific result are very wide.

The effects of radiation on Tl-based systems have both scientific depth and shortcomings.

In particular, concerning Warburg impedance, the observed enhancement in ion mobility is reflected in an increased Warburg contribution within the impedance spectra. Since the impedance of these materials is directly influenced by the absorbed radiation dose, they exhibit potential for application in the development of next-generation dosimeters.

Moreover, the irradiation-induced improvement in the conductivity of solid electrolytes can contribute to a reduction in the internal resistance of batteries used in micro-electro-mechanical systems.

Acknowledgement: Not applicable.

Funding Statement: The authors received no specific funding for this study. The APC payment for the article will be covered by the authors.

Author Contributions: The authors confirm contribution to the paper as follows: Study conception and design: A. A. Orujova. Data collection: A. A. Orujova, R. Sh. Agayeva. Analysis and interpretation of results: N. I. Guliyev, T. F. Yusibova. Draft manuscript preparation: R. Sh. Agayeva, G. A. Ismayilbeyli, N. I. Guliyev. All authors reviewed and approved the final version of the manuscript.

Availability of Data and Materials: The data supporting the findings of this study are available from the corresponding author upon reasonable request.

Ethics Approval: Not applicable.

Conflicts of Interest: The authors declare no conflicts of interest.

References

1. Vogt T. Layered semiconductors: Structure and properties. J Solid State Chem. 2020;289:121406. [CrossRef].
2. Popescu M. Electrical conductivity of $TlGaSe_2$ crystals. Mater Res Bull. 2019;111:250–57. [CrossRef].
3. Sidebottom DL. *Colloquium*: Understanding ion motion in disordered solids from impedance spectroscopy scaling. Rev Mod Phys. 2009;81(3):999–1014. [CrossRef].
4. Huang Y, Shih H, Mansfeld F. Concerning the use of constant phase elements (CPEs) in the analysis of impedance data. Mater Corros. 2010;61(4):302–5. [CrossRef].
5. Jorcin JB, Orazem ME, Pébère N, Tribollet B. CPE analysis by local electrochemical impedance spectroscopy. Electrochim Acta. 2006;51(8–9):1473–9. [CrossRef].
6. Doi A. Comment on Warburg impedance and related phenomena. Solid State Ion. 1990;40:262–5. [CrossRef].
7. MacDonald JR. Impedance spectroscopy: Old problems and new developments. Electrochim Acta. 1990;35(10):1483–92. [CrossRef].
8. Nikonenko VV, Kozmai AE. Electrical equivalent circuit of an ion-exchange membrane system. Electrochim Acta. 2011;56(3):1262–9. [CrossRef].
9. Bobnar V, Lunkenheimer P, Paraskevopoulos M, Loidl A. Separation of grain boundary effects and intrinsic properties in perovskite-like $Gd_{0.6}Y_{0.4}BaCo_2O_{5.5}$ using high-frequency dielectric spectroscopy. Phys Rev B. 2002;65(18):184403. [CrossRef].
10. Vasil'ev RB, Dorofeev SG, Rumyantseva MN, Ryabova LI, Gas'kov AM. Impedance spectroscopy of ultrafine-grain SnO_2 ceramics with a variable grain size. Semiconductors. 2006;40(1):104–7. [CrossRef].
11. Liu ZG, Ouyang JH, Sun KN, Zhou Y. Electrical conductivity of 5 mol.% Yb_2 O_3 and 5mol.% Gd_2O_3 co-doped $Sm_2Zr_2O_7$. Mater Lett. 2011;65(2):385–7. [CrossRef].
12. Lunkenheimer P, Bobnar V, Pronin AV, Ritus AI, Volkov AA, Loidl A. Origin of apparent colossal dielectric constants. Phys Rev B. 2002;66(5):052105. [CrossRef].
13. Adams TB, Sinclair DC, West AR. Characterization of grain boundary impedances in fine- and coarse-grained $CaCu_3Ti_4O_{12}$ ceramics. Phys Rev B. 2006;73(9):094124. [CrossRef].
14. Kumar Jana P, Sarkar S, Chaudhuri BK. Maxwell–Wagner polarization mechanism in potassium and titanium doped nickel oxide showing giant dielectric permittivity. J Phys D Appl Phys. 2007;40(2):556. [CrossRef].
15. Chern G, Song LR, Shi JB. Observation of high dielectric permittivity in single-crystal $Bi_2Sr_2CoO_{6+\delta}$. Phys C Supercond. 1995;253(1–2):97–101. [CrossRef].
16. Mazzara G, Skirius S, Cao G, Chern G, Clark R, Crow J, et al. High dielectric permittivity of ceramic and single-crystal $PrBa_2Cu_3O_x$. Phys Rev B. 1993;47(13):8119–23. [CrossRef].
17. Ramirez AP, Subramanian MA, Gardel M, Blumberg G, Li D, Vogt T, et al. Giant dielectric constant response in a copper-titanate. Solid State Commun. 2000;115(5):217–20. [CrossRef].
18. Rey C, Mathias H, Testardi L, Skirius S. High dielectric constant and nonlinear electric response in nonmetallic $YBa_2Cu_3O_{6+\delta}$. Phys Rev B. 1992;45(18):10639–46. [CrossRef].
19. Samara G, Hammetter W, Venturini E. Temperature and frequency dependences of the dielectric properties of $YBa_2Cu_3O_{6+x}$. Phys Rev B. 1990;41(13):8974–80. [CrossRef].
20. Subramanian MA, Li D, Duan N, Reisner BA, Sleight AW. High dielectric constant in $ACu_3Ti_4O_{12}$ and $ACu_3Ti_3FeO_{12}$ phases. J Solid State Chem. 2000;151(2):323–5. [CrossRef].
21. Bin Arif SM, Saleem M, Quader A, Munir O, Rasheed A, Shakoor A, et al. Integration of W into NiSe as a novel and efficient electrode material with superior energy storage capabilities for supercapacitors. J Power Sources. 2026;662:238765. [CrossRef].
22. Adediwura SC, Mathew N, auf der Günne JS. Combining NMR and impedance spectroscopy in situ to study the dynamics of solid ion conductors. J Mater Chem A. 2024;12(26):15847–57. [CrossRef].
23. Matkin DE, Starostina IA, Hanif MB, Medvedev DA. Revisiting the ionic conductivity of solid oxide electrolytes: A technical review. J Mater Chem A. 2024;12(38):25696–714. [CrossRef].
24. Doughri D, Mehdaoui B, Fakhreddine R, El Bouari A. Structural, dielectric and ac ionic conductivity of Li_4FeSbO_6 oxide. Mater Chem Phys. 2024;318:129310. [CrossRef].

25. Samal S, Mishra S, Parida SK. Microstructure, dielectric, and impedance spectroscopy of the dysprosium-modified $LaBiO_3$ ceramic. Ferroelectrics. 2024;618(2):321–33. [CrossRef].
26. Yadav AK, Pandey R, Singh P. Impedance spectroscopy in perovskite materials: From fundamentals to applications. Inorg Chem Commun. 2025;182:115524. [CrossRef].